Appl Phys B
DOI 10.1007/s00340-011-4442-2

Applied Physics B
Lasers and Optics

Intracavity system design for IR multiphoton dissociation

V.M. Freytes · J. Codnia · M.L. Azcárate

Received: 28 July 2010 / Revised version: 28 January 2011

Abstract An intracavity system for the infrared multiple photon dissociation (IRMPD) of molecules with high dissociation energy threshold has been designed and implemented. The system design based on a TEA CO_2 laser with a cavity folded in V-shape included the analysis of its stability varying the cavity dimensions as well as the analysis of the positions of the beam waists and of the beam size at them. The intracavity energy as a function of the total sample pressure has been measured and the laser-operation threshold has been determined. Intracavity IRMPD has been compared to traditional IRMPD performed in an irradiation geometry in which the radiation is focused into a photoreactor placed outside the laser cavity. Dissociation volumes in intracavity irradiation have resulted an order of magnitude larger than those obtained in experiments performed with the photoreactor outside the laser cavity.

1 Introduction

The growing interest in isotopically pure materials has directed attention toward the development of new isotope separation techniques. One extensively studied technique is based on a selective photochemical process: the infrared multiple photon dissociation (IRMPD) of polyatomic molecules. In a strong IR field coincident with one of its vibrational bands, a polyatomic molecule will sequentially absorb IR photons and accumulate enough energy to dissociate [1–3]. The IRMPD involves an efficient use of the energy since it is only deposited in the isotope that is to be separated. Thus, this technique is a particularly useful tool to separate less abundant isotopes.

The implementation of this technique requires the selection of an adequate "working molecule" as well as of the irradiation geometry including the laser and the photoreactor to dissociate the largest number of molecules per pulse at the highest pressure compatible with energy-transfer processes.

Thus, the design of laser-photoreactor systems for the optimization of the IRMPD technique poses some questions. On one hand, highly focused geometries are of great use when it is necessary to increase the energy per unit area, defined as fluence, in the IRMPD of molecules with high dissociation energy threshold. However, the dissociation volumes achieved in these systems are small and, therefore, the global process efficiency decreases. In previous works, we have obtained more uniform energy distributions in the photoreactor using less focused geometries [4, 5] and, in consequence, larger irradiation volumes have resulted. Nevertheless, in many cases, it is not possible to achieve high fluence values and, hence, the effective volume of dissociation remains reduced. In order to increase the effective volume of dissociation it is therefore desirable to work with high fluence, i.e. with high energy, in large volumes. High irradiation energy can be obtained in passive (external resonator) and active (laser resonator) intracavity systems [6].

An intracavity intensity much larger than incident can be obtained in an external resonator with high reflecting mirrors

V.M. Freytes (✉) · J. Codnia · M.L. Azcárate
CEntro de Investigaciones en Láseres y APlicaciones (CEILAP), Instituto de Investigaciones Científicas y Técnicas para la Defensa (CITEDEF—CONICET), J. B. de La Salle 4397 (B160ALO), Villa Martelli, Argentina
e-mail: mfreytes@conicet.gov.ar
Fax: +54-11-47098100

J. Codnia
e-mail: jcodnia@citedef.gob.ar

M.L. Azcárate
e-mail: lazcarate@citedef.gob.ar

V.M. Freytes · M.L. Azcárate
Carrera del Investigador CONICET, Buenos Aires, Argentina

Published online: 26 February 2011

as a consequence of the coherent superposition of the multiple reflections of the radiation. Various orders of magnitude intensity amplification can be achieved with this system but only for small sample absorption ($\alpha L \ll 1$, α sample absorption coefficient, L photoreactor length). An additional drawback is that, in order to match the laser and the external resonators modes in high finesse conditions, cavity length control systems of one of the resonators are required.

Active intracavity systems with weak absorbing gases have been widely spread for absorption spectroscopy and trace gases detection studies [7]. In most of these works the energy loss due to absorption is negligible with regard to the intrinsic resonator losses and the aim is to improve the sensitivity of the detection. Large sensitivity enhancement is obtained when the signal detected is proportional to the intensity such as with the laser induced fluorescence and photothermal techniques [6]. Active intracavity systems are versatile enough and even in strong absorption conditions the sample parameters such as the absorption coefficient or concentration can be inferred from the measurement of the laser output power [6, 8].

On the other hand, active intracavity systems for dissociation have been scarcely studied. Lockman et al. [9] have implemented an intracavity system with a TEA CO_2 laser for the IRMPD of CF_2Cl_2. Since the dissociation energy of this molecule is quite low, it was not necessary to focus the radiation and the system behaved as a linear plano-concave cavity. Although these types of systems are useful for molecules with low dissociation energy, it is necessary to develop systems to optimize the radiation incident on molecules with high energy dissociation threshold such as $CDCl_3$ [10–13].

These considerations led us to design and implement an active intracavity system to improve the use of the laser energy in the IRMPD of molecules with high dissociation energy threshold. This system allows a higher energy density to be obtained in a larger volume in the photoreactor than in a single-pass outside the cavity. But when $\alpha L \ll 1$ is not satisfied, the absorption losses introduced in the laser cavity produce significant changes in the laser parameters. However, the system implemented takes advantage of the large small signal gain of the TEA CO_2 laser. In a cavity with high reflectivity mirrors, the main loss will be the sample absorption. If the total losses are kept lower than the small signal gain, the laser will still work building up in each round trip the energy consumed by absorption.

In this work the system performance with the absorbent gas was first analyzed. Then, the intracavity energy as a function of the total pressure of a pre-enriched isotopic sample was measured and the laser-operation threshold was determined. Finally, the intracavity IRMPD of 1% $CDCl_3$ in $CHCl_3$ was performed. The results obtained with this system were compared with those obtained in traditional irradiation geometry with the radiation being focused into a photoreactor placed outside the laser cavity.

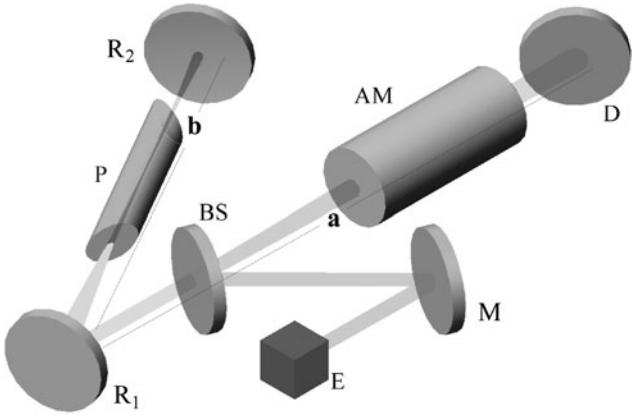

Fig. 1 Sketch of the experimental set-up of the IRMPD intracavity system. *P*: photoreactor, R_1 and R_2: mirrors of focal distances focal f_1 and f_2, respectively, *D*: diffraction grating, *BS*: beam-splitter, *AM*: laser active medium, *M*: mirror, *E*: energy meter

2 Experimental set-up

2.1 Intracavity system design

A homemade TEA CO_2 laser with a cavity folded in V-shape formed by a diffraction grating and two concave mirrors was used for the system implementation. In the branch limited by the diffraction grating and one of the mirrors (R_1), branch of length a in Fig. 1, the beam waist is located on the diffraction grating as in the case of a plano-concave cavity. In the other branch limited by the two curved mirrors (R_1 and R_2), branch of length b in Fig. 1, the beam waist is located in a point between both mirrors. This configuration allows the photoreactor to be placed in branch b of the cavity and to position it so as to focus the radiation in its center as shown in Fig. 1.

Different factors have been taken into account for the design of the V-shape cavity: its stability, the location of the beam waist in the branch of length b and the beam size on the mirrors and on the photoreactor's windows.

The control of the beam diameter at different points of the cavity allows, on one hand, to maximize the fluence in the center of the photoreactor and, on the other, to obtain fluence values lower than the damage threshold at the mirrors and the windows. In order to carry out this design the dependence of these factors on the length of the branches and on the curvature radii of the mirrors was analyzed. These studies were made using the formalism ABCD for matrices [14] as well as the formalism of Gaussian beams propagation [14] corrected by the beam quality factor, M^2, [15] for non-Gaussian beams. The analysis performed resulted in expressions for the position of the beam waist, z_f^b, the Rayleigh range, z_R^b, defined as the length for which the beam size at the focus increases by a factor $\sqrt{2}$ [14], and the beam sizes at the mirrors and in the waist, w_1, w_2 and w_f, respectively,

in the branch of length b:

$$z_f^b = \frac{(f_2 + y)(f_1^2 - xy - xf_2)}{f_1^2 - 2xy}, \tag{1}$$

$$z_R^b = \frac{\sqrt{f_2^2 - y^2}}{f_1^2 - 2xy}\sqrt{(f_1^2 - xy)^2 - x^2 f_2^2}, \tag{2}$$

$$w_1 = \sqrt{\frac{\lambda z_R^b}{\pi} M^2 \left(1 + \left(\frac{f_1 + f_2 + y - z_f^b}{Z_R^b}\right)^2\right)}, \tag{3}$$

$$w_2 = \sqrt{\frac{\lambda z_R^b}{\pi} M^2 \left(1 + \left(\frac{z_f^b}{z_R^b}\right)^2\right)}, \tag{4}$$

$$w_f = \sqrt{\frac{\lambda z_R^b}{\pi} M^2} \tag{5}$$

where f_1 and f_2 are the focal lengths of mirrors R_1 and R_2 (Fig. 1), respectively, and the implicit definitions of the lengths x and y are $a = f_1 + x$ and $b = f_1 + f_2 + y$.

The cavity was designed so that the position of the focal point in the branch of length b would not depend on length a. The choice of $y = f_2$ in (1) results in $z_f^b = 2y$, which does not depend on x and, thus, on a. If f_1 and f_2 are defined such that $f_1 = mf_2 = mf$ ($m \in \Re$) and with the requisite that the beam waist must be near the center of branch b, that is, $z_f^b \sim b/2, m = 2$ and $b \sim 4f$ result. These conditions set the system at the stability border, and therefore, z_R^b and, consequently, w_1, w_2 and w_f, vary strongly with length b when $b \sim 4f$. This effect is critical during the alignment process of the system.

2.2 Intracavity IRMPD experiments

The TEA CO_2 laser cavity folded in V-shape with the photoreactor inside one branch was implemented. Photoreactor for intracavity placement was made on Pyrex glass and T-shaped (92 cm and 150 cm long and 2 cm diameter with arms of the same diameter and 7 cm long each) to enable FTIR spectra to be registered to determine the sample composition before and after irradiation. Inside the cavity ZnSe windows were sealed at Brewster angle to minimize laser losses. KCl windows were used for FTIR analysis.

The mirrors and length b of the V-shaped cavity were chosen so that the laser would operate in the stable region and the beam waist be located in the middle of branch b independently of length a. This was obtained with a diffraction grating (150 l/mm) which allows the laser to be tuned in the 9–11 μm range and two concave mirrors of 100% reflectivity and focal distances $f_1 = 50$ cm and $f_2 = 100$ cm. A diagram of the experimental set-up is shown in Fig. 1.

A ZnSe beam-splitter was placed between the photoreactor and mirror R_1 in branch a. This beam-splitter had been previously characterized by analyzing the dependence of its transmittance and reflectivity on the angle formed with the cavity axis. As it can be observed in Fig. 1, the beam emerging from the beam-splitter is deviated to an energy meter (Gen-Tec, ED 200) by a mirror, M. The laser emission line was verified with a CO_2 laser spectrum analyzer (Optical Engineering Inc.), which was set instead of the energy meter in the same place. Likewise, the intracavity system alignment was performed with a He-Ne laser incident on the beam-splitter. Alternatively, the intracavity energy was measured sensing the leak at the cero order of the diffraction grating without the beam-splitter.

Mixtures of 0.26% and 1% $CDCl_3$ in $CHCl_3$ were used as the absorbent gas. The laser was tuned to the 10P(48), 916.7 cm^{-1}, emission line, which is resonant with the $CDCl_3$ ν_4 vibrational mode (913.9 cm^{-1}) [16]. The reagents used were $CDCl_3$ (Merck), 99.98% and $CHCl_3$ (Merck), 99.9%. $CHCl_3$ was distilled in order to remove the stabilizer. The sample pressure was varied between 1 and 15 Torr in intracavity configuration.

The sample partial pressure before and after each irradiation was determined by IR spectrometry with an IR Fourier Transform (FTIR) spectrometer (Perkin Elmer, System 2000). In order to improve the signal-to-noise ratio, each spectrum was obtained from 40 scans registered with a resolution of 1 cm^{-1}. The dissociation progress was followed recording spectra every 50 pulses in order to obtain significant variations in the reactant and products concentrations. The reactants and products composition in each spectrum was determined using calibrated spectra of the different gases and a program based on non-linear regression techniques.

3 Results and discussion

3.1 Laser response in intracavity configuration

The intracavity system was implemented and the intracavity energy varying the sample pressure was measured in the first place. Figure 2 shows the dependence of the intracavity energy on the total sample pressure when the absorbent gas consisted of a mixture of 0.26% $CDCl_3$ in $CHCl_3$. It can be observed that the laser energy decreases as the absorbent gas pressure increases and, for pressures in the photoreactor larger than 15 Torr, the laser stops working.

The intensity variation inside the cavity was analyzed with a Rygrod [14] type analysis in order to explain the operation limit of the laser. The effects of the mirrors R_1 and R_2, the diffraction grating, the windows of the photoreactor and of the active medium and the beam-splitter were accounted for through their respective transmittances, τ_i, and reflectances, r_i.

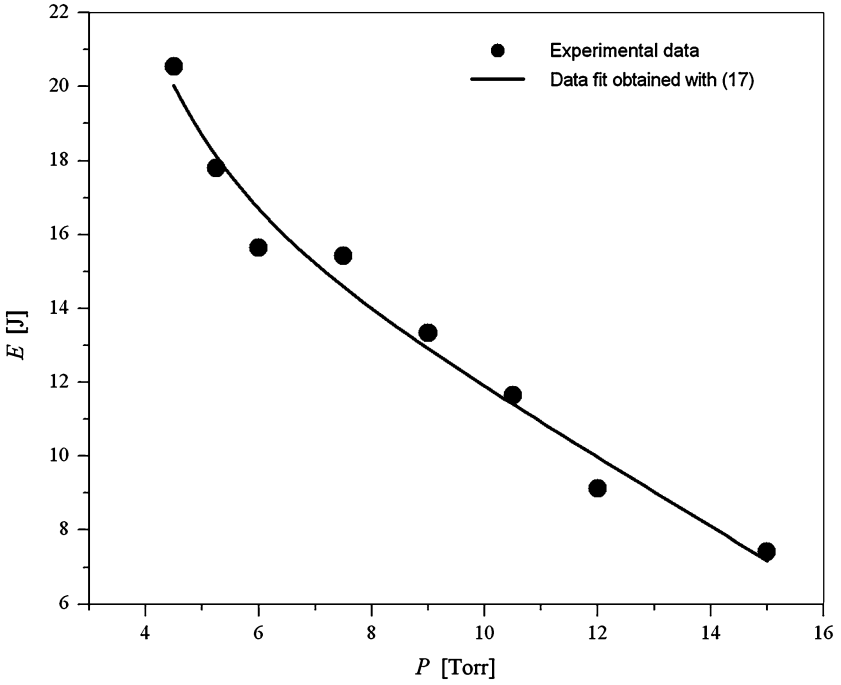

Fig. 2 Dependence of laser energy, E, on total sample pressure, P, for a mixture of 0.26% de $CDCl_3$ in $CHCl_3$ in a photoreactor 150 cm long. The *solid line* is the data fit obtained with (17)

The effects of the active medium of length L_0 and of the absorbent medium of length L were analyzed considering that the intensity of the wave passing through them will increase or decrease with distance according to the differential equation [14]:

$$\frac{dI}{dz} = \pm \alpha_I I \tag{6}$$

where the sign + or −, corresponds to a medium with gain as in the case of a laser, or a medium with losses as in the case of the absorbent gas, respectively. The parameter α_I is the gain or absorption coefficient of the medium.

In the active medium the gain coefficient will saturate as the intensity increases as [14]

$$\alpha_I = \frac{\alpha}{1 + I/I_{\text{sat}}} \tag{7}$$

where α is defined as the small signal gain and I_{sat} is the saturation intensity of the gain. For simplicity, the intensity I in any region of the cavity is normalized to the I_{sat} intensity defining:

$$\beta = I/I_{\text{sat}} \tag{8}$$

In the case of an absorbent medium, the intensity change inside the photoreactor according to (6), β_{ph}, will be given by

$$\frac{1}{\beta_{\text{ph}}} \frac{d\beta_{\text{ph}}}{dz} = -\Gamma \tag{9}$$

where Γ depends on the working molecule and on the sample pressure. The photoreactor transmittance, χ, can be therefore defined in the following way:

$$\chi = \frac{\beta_{\text{out}}}{\beta_{\text{in}}} = e^{-\Gamma L} \tag{10}$$

where the subscripts in and out correspond to the incident and emerging intensities of the photoreactor, respectively. From these considerations and from the ratios of the transmitted to the reflected intensity in the optical components of the cavity it is possible to obtain the expression for β in any place of the cavity.

The intensity inside the photoreactor can be expressed as

$$\beta_{\text{ph}} = \frac{\alpha L_0 + \ln(r_1 \tau_{\text{BS}} \chi \tau_V^4 \sqrt{r_2 r_R})}{1 - r_1 \tau_{\text{BS}} \tau_V^4 \chi \sqrt{r_2 r_R}} \frac{r_1 \tau_{\text{BS}} \tau_V^2 \chi \sqrt{r_R}}{r_1 \tau_{\text{BS}} \tau_V^2 \chi \sqrt{r_2} + \sqrt{r_R}} \times \left(e^{-\Gamma(z-L)} + \tau_V^2 r_2 e^{\Gamma(z-L)}\right) \tag{11}$$

where r_1, r_2 and r_R are the reflectivities of the mirrors R_1, R_2 and of the diffraction grating, RD, respectively (Fig. 1); τ_V, τ_{BS}, are the transmittances of the photoreactor windows and of the beam-splitter, respectively, and, L and L_0 are the photoreactor and active medium lengths, respectively.

The intensity in the center of the photoreactor ($z = 0$) results from (11):

$$\beta_{\text{ph}} = \frac{\alpha L_0 + \ln(r_1 \tau_{\text{BS}} \chi \tau_V^4 \sqrt{r_2 r_R})}{1 - r_1 \tau_{\text{BS}} \tau_V^4 \chi \sqrt{r_2 r_R}} \frac{r_1 \tau_{\text{BS}} \tau_V^2 \sqrt{r_R}}{r_1 \tau_{\text{BS}} \tau_V^2 \chi \sqrt{r_2} + \sqrt{r_R}} \times \left(1 + \tau_V^2 r_2 \chi^2\right) \tag{12}$$

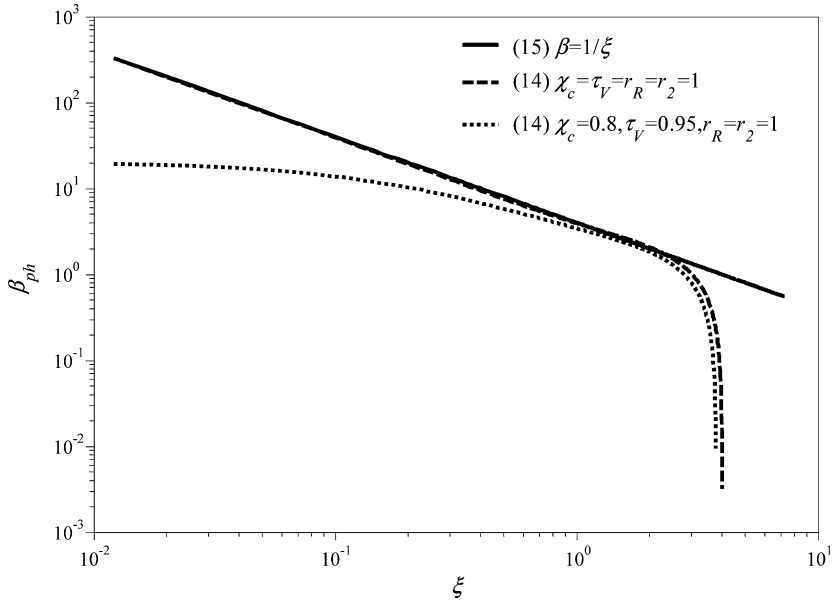

Fig. 3 Normalized absorption in the photoreactor, β_{ph}, vs. sample absorption, $\xi = n\sigma L$, assuming $\alpha L_0 = 4$

Defining χ_c as

$$\chi_c = r_1 \tau_{\mathrm{BS}} \tau_V^4 \sqrt{r_2 r_R} \tag{13}$$

one obtains

$$\beta_{\mathrm{ph}} = \frac{\alpha L_0 + \ln(\chi\chi_c)}{1 - \chi\chi_c} \frac{\sqrt{r_R}}{\sqrt{r_2}} \frac{\chi_c}{r_R + \chi\chi_c} \left(1 + \tau_V^2 r_2 \chi^2\right) \tag{14}$$

The gas absorbance can be described as $\xi = \Gamma L = n\sigma L$, where n is the sample concentration in molecules cm^{-3} and σ is the absorption cross-section in cm^2 $\mathrm{molecules}^{-1}$. Therefore, the photoreactor transmittance results $\chi = e^{-\xi}$. Assuming that the only losses are those produced by the gas absorption in the photoreactor, $\chi_c = 1$, and that the absorption is low, $\xi \ll 1$,

$$\beta_{\mathrm{ph}} \approx \frac{\alpha L_0 - \xi}{\xi} \approx \frac{1}{\xi} \tag{15}$$

The dependence of the normalized absorption in the photoreactor, β_{ph}, on the sample absorption, ξ, which is directly proportional to the concentration, n, is shown in Fig. 3. The curves in the graph have been calculated with expressions (14) and (15) with $\alpha L_0 = 4$, which is a typical value for TEA CO_2 lasers [17]. Two cases have been considered for expression (14): (1) the losses are produced only by absorption, $\chi_c = \tau_V = r_R = r_2 = 1$ and (2) there are additional losses such that $\chi_c = 0.8$, $\tau_V = 0.95$ and $r_R = r_2 = 1$. In the first case, for low concentrations of the absorbent sample the intensity in the photoreactor decreases with increasing concentration (or the sample pressure). For sample pressure values near the laser-operation threshold, the absorption effect is even more pronounced. Near the laser-operation threshold the intensity is very low and lasing in all pulses is not obtained as a consequence of small pulse-to-pulse fluctuations in the laser gain. In the second case, three regimes are observed. At low absorbent concentration ($\xi \ll 1$) the effect of the losses in the cavity is much larger than the effect of the sample absorption and the intensity in the photoreactor is considerably lower than in the case where no losses in the cavity were considered. A second regime is appreciated when the absorption exceeds the cavity losses. As can be seen in Fig. 3, the curves tend to merge since in this case the predominant effect is the absorption in the photoreactor. Finally, in the third regime, the absorption is so important that the intensity strongly falls reaching the laser-operation limit.

This model was then used to fit the experimental data of the dependence of the intracavity laser energy on the total pressure of the absorbent gas obtained with a mixture of 0.26% $CDCl_3$ in $CHCl_3$ in a 150 cm long photoreactor. Considering the relationship between the absorbance, ξ, and the sample pressure, P:

$$\xi = n\sigma L = 3.22 \times 10^{16} P \sigma L \tag{16}$$

Equation (14) can be expressed in terms of the measured intracavity energy:

$$E_{\mathrm{int}ra} = C \frac{\alpha L_0 + \ln(\chi_c) - \xi}{1 - \chi_c e^{-\xi}} \frac{\sqrt{r_R}}{\sqrt{r_2}} \frac{\chi_c}{\tau_V^2 r_R + e^{-\xi}\chi_c} \times \left(1 + \tau_V^2 r_2 e^{-2\xi}\right) \tag{17}$$

where the constant, C, accounts for the energy units and the factor corresponding to the ratio of the energy inside the photoreactor to the energy measured in any point of the cavity. This fit was performed considering only the losses at

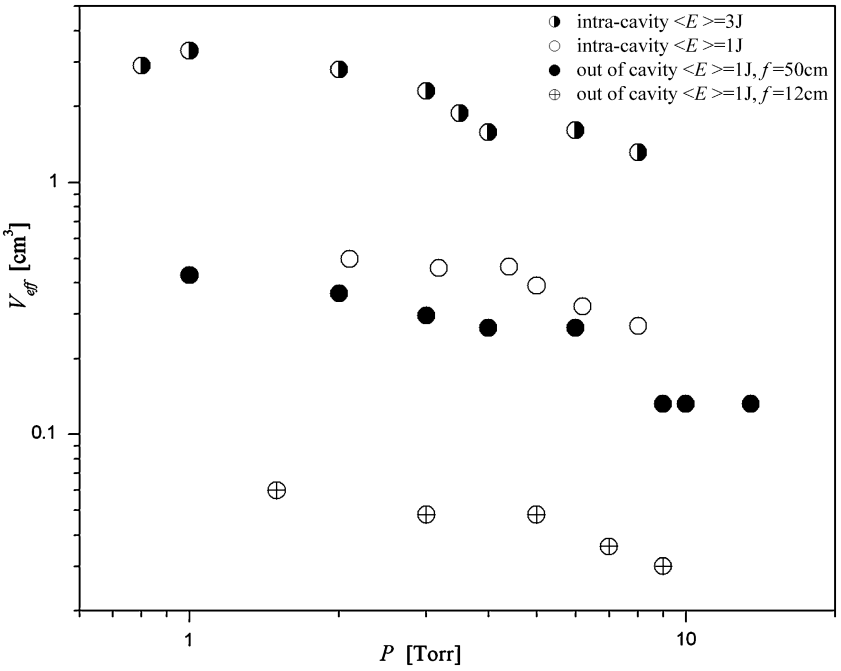

Fig. 4 Dependence of the effective dissociation volume, V_{eff}, on the total sample pressure, P. Comparison of results of the experiments performed in intracavity configuration with those obtained in irradiation geometry outside the laser cavity

Table 1

C (J)	αL_0	σ_{eff} (cm^2 molec^{-1})
3.69	5.60	5.0×10^{-20}

the windows of the photoreactor and at the diffraction grating, $\tau_v = 0.98$ and $r_R = 0.9$. Losses at the mirrors were not taken into account so that $r_1 = r_2 = 1$, and since the beamsplitter was no used, thus, $\tau_{\text{BS}} = 1$. An excellent agreement between the experimental data and those calculated with expression (17) can be observed in Fig. 2 and the resulting parameters are shown in Table 1. The values obtained are consistent with those expected considering typical values of $\alpha L_0 \geq 3$ for a TEA CO_2 laser [17] and about 10^{-20} cm^2 molecule^{-1} for σ_{eff} [18]. σ_{eff} is the absorption cross-section of $CDCl_3$ and $CHCl_3$ mixtures given by

$$\sigma_{\text{eff}} = \frac{\sigma_{\text{CHCl}_3}}{1 + Ri}\left(1 + \frac{\sigma_{\text{CDCl}_3}}{\sigma_{\text{CHCl}_3}} Ri\right) \tag{18}$$

where σ_{CDCl_3} and σ_{CHCl_3} are the absorption cross-sections of the $CDCl_3$ and $CHCl_3$ isotopomers, respectively, and Ri is the isotopic ratio of the sample.

3.2 $CDCl_3$ IRMPD in the intracavity system

Finally, $CDCl_3$ IRMPD experiments were performed in mixtures of 1% $CDCl_3$ in $CHCl_3$ in the intracavity photoreactor 93 cm long and the results were compared with those obtained in experiments preformed with the same mixture in focused irradiation geometry outside the laser cavity.

The fraction of dissociated molecules, f_N^d, was calculated from the $CDCl_3$ concentration before and after irradiation as follows:

$$f_N^d = \frac{[\text{CDCl}_3]_N}{[\text{CDCl}_3]_0} \tag{19}$$

where N is the number of pulses. The fraction of dissociated molecules per pulse, f^d, was calculated from the f_N^d vs. N curve and the effective dissociation volume, V_{eff}, was obtained as the product of f^d and the photoreactor volume, V_f:

$$V_{\text{eff}} = f^d V_f \tag{20}$$

Figure 4 shows a comparative graph of the effective dissociation volume vs. total sample pressure curves obtained in intracavity and in focused geometry outside the laser cavity experiments. The results obtained in intracavity experiments with two different mean irradiation energies, 1 J and 3 J, are presented. In the focused geometry outside the laser cavity experiments the mean laser output energy was 1 J.

The values of the effective dissociation volume, V_{eff}, obtained in intracavity configuration with the laser operating at 1 J, although somewhat higher, are of the same order as those obtained with a similar focusing geometry, $f = 50$ cm, outside the cavity. Higher energies than those obtained in irradiations outside the cavity were achieved with the intracavity system. An increase of one order of magnitude of the V_{eff} values was obtained with the laser operated at 3 J. This V_{eff} increase was the result of the fluence increase in the whole volume of the photoreactor due to the larger available energy.

4 Conclusions

An intracavity system for the IRMPD of molecules with high dissociation energy threshold has been designed and implemented. A TEA CO_2 laser with a cavity folded in V-shape was used. The design of the laser to operate in this configuration included the analysis of its stability varying the cavity dimensions as well as the analysis of the positions of the beam waists and of the beam size at them. This analysis enabled the choice of the most suitable configuration to satisfy the focusing requirements in the photoreactor. These were a high dissociation probability in a large volume and, at the same time, beam sizes at the windows of the photoreactor and at the cavity mirrors big enough so that the fluence would no exceed their damage threshold.

A theoretical-experimental study of the intracavity energy variation has been performed. This analysis enabled the dependence of the energy variation on the absorbent gas concentration to be modeled. An excellent agreement between the proposed model and the experimental data obtained in $CDCl_3$ and $CHCl_3$ mixtures has been obtained. It has been found that the laser operation is conditioned by the inclusion of the photoreactor with the absorbent gas inside the cavity. This intracavity absorbent medium introduces a loss that affects the laser intensity and, once a certain threshold is overcome, the laser stops working. It has been found, too, that for the laser and the absorbent gas used this threshold is overcome for pressures larger than 15 Torr. It has been determined that the laser operation threshold strongly depends on its gain, on the sample absorption and, to a less extent, on the cavity losses other than the absorption.

Finally, experiments of IRMPD of $CDCl_3$ in intracavity configuration have been performed varying the $CDCl_3$ pressure and the irradiation energy. The dependence of the fraction of dissociated molecules per pulse and the corresponding effective dissociation volume on sample pressure with irradiation energies of 1 and 3 J has been determined. The results have been compared with those obtained in experiments performed in a focused geometry outside the laser cavity. Similar values have been obtained with similar energies and focusing conditions in both configurations. Values of the fraction of molecules dissociated per pulse an order of magnitude higher have been obtained with irradiation energy of 3 J in intracavity configuration.

It can be concluded that intracavity systems such as those implemented in this work largely improve the IRMPD schemes for molecules with high dissociation threshold energy due to the optimization of the use of the laser available energy.

References

1. V.S. Letokhov, *Multiple-Photon Excitation and Dissociation of Polyatomic Molecules* (Springer, Berlin, Heidelberg, 1986)
2. O.V. Boyarkin, M. Kowalzcyk, T.R. Rizzo, J. Chem. Phys. **118**, 93 (2003)
3. J. Makowe, Isotopically selective infrared multiphoton dissociation of vibrationally pre-excited silane, PhD thesis, Ecole Polytechnique Federale de Lausanne, 2004
4. V.M. Freytes, Disociación multifotónica IR de isótopos de interés tecnológico, PhD thesis, FCEyN—UBA, 2006
5. J. Codnia, V.M. Freytes, M.L. Azcárate, An. AFA **17**, 94 (2005)
6. W. Demtröder, *Laser Spectroscopy* (Springer, Berlin, Heidelberg, New York, 1996)
7. V.M. Baev, T. Latz, P.E. Toschek, Appl. Phys. B **69**, 171 (1999)
8. Al-Hawat, Opt. Lasers Eng. **46**, 380 (2008)
9. V.N. Lokhman, G.N. Makarov, E.A. Ryabov, M.V. Sotnikov, Quantum Electron. **26**, 79 (1996)
10. F. Magnotta, I.P. Herman, F.T. Aldridge, Chem. Phys. Lett. **92**, 600 (1982)
11. I.P. Herman, F. Magnotta, R.J. Buss, Y.T. Lee, J. Chem. Phys. **79**, 1789 (1983)
12. M.L. Azcárate, E.J. Quel, Appl. Phys. B **47**, 239 (1988)
13. M.L. Azcárate, E.J. Quel, Appl. Phys. B **47**, 223 (1988)
14. A.E. Siegman, *Lasers* (University Sciences Books, Mill Valley, 1986)
15. A.E. Siegman, S.W. Townsend, IEEE J. Quantum Electron. **29**, 1212 (1993)
16. T. Shimanouchi, Tables of Molecular Vibrational Frecuencies, vol. II. Natl. Bur. Stand., 1972
17. W.J. Witteman, *The CO_2 Laser* (Springer, Heidelberg, Berlin, 1987)
18. M.L. Azcárate, Procesos multifotónicos IR en $CDCl_3$ inducidos por láser de CO_2, PhD thesis, FCEyN—UBA, 1986